J. Condensed Matter Nucl. Sci. 38 (2024) 196–210

Research Article

The Case of the Missing Tritium

Pamela A. Mosier-Boss*, Lawrence P. Forsley

Global Energy Corporation, USA

Abstract

Pd/D co-deposition experiments conducted in low and high tritiated D_2O are discussed. Four different groups, using different cathodes, electrolytes, and methodologies, performed these experiments. It was observed that when low tritiated D_2O was used, tritium was produced. However, a loss of tritium occurred when highly tritiated D_2O was employed. In this communication we explore the reactions and mechanisms that could explain this loss of tritium.
 ISSN 2227-3123

Keywords: Tritium, Pd/D co-deposition, electron screening, cross-sections, nanoparticles

1. Introduction

In the Pd/D co-deposition process, Pd is plated out onto a cathode substrate in the presence of evolving deuterium gas [1]. This results in an ever-expanding electrode surface consisting of Pd microglobules that instantly load with deuterium. Using variations of Pd/D co-deposition, researchers have reported on observing excess heat, γ- and X-ray emissions, transmutation, as well as the generation of energetic particles. Four groups of researchers have conducted Pd/D co-deposition experiments that focused on tritium production [2]–[6]. These researchers used different cathode substrates, plating solutions, and methodologies. Regardless of the experimental procedure employed, an increase in tritium was observed when low-tritiated D_2O was used, and a decrease occurred when highly tritiated D_2O was used. The decrease in tritium observed when highly tritiated D_2O was used suggests that there is a nuclear reaction(s) occurring inside the Pd lattice that consumes tritium. This loss of tritium is not observed when bulk Pd is used implying that the reaction(s) involved with the consumption of tritium is related to the high surface area of the Pd deposit and/or the vacancies present in the lattice [1]. In this communication we explore the possible reactions of tritium with Pd and Li isotopes as well as energetic particles to determine what reaction(s) can account for this loss.

*Corresponding author: pboss@san.rr.com

 ISSN 2227-3123

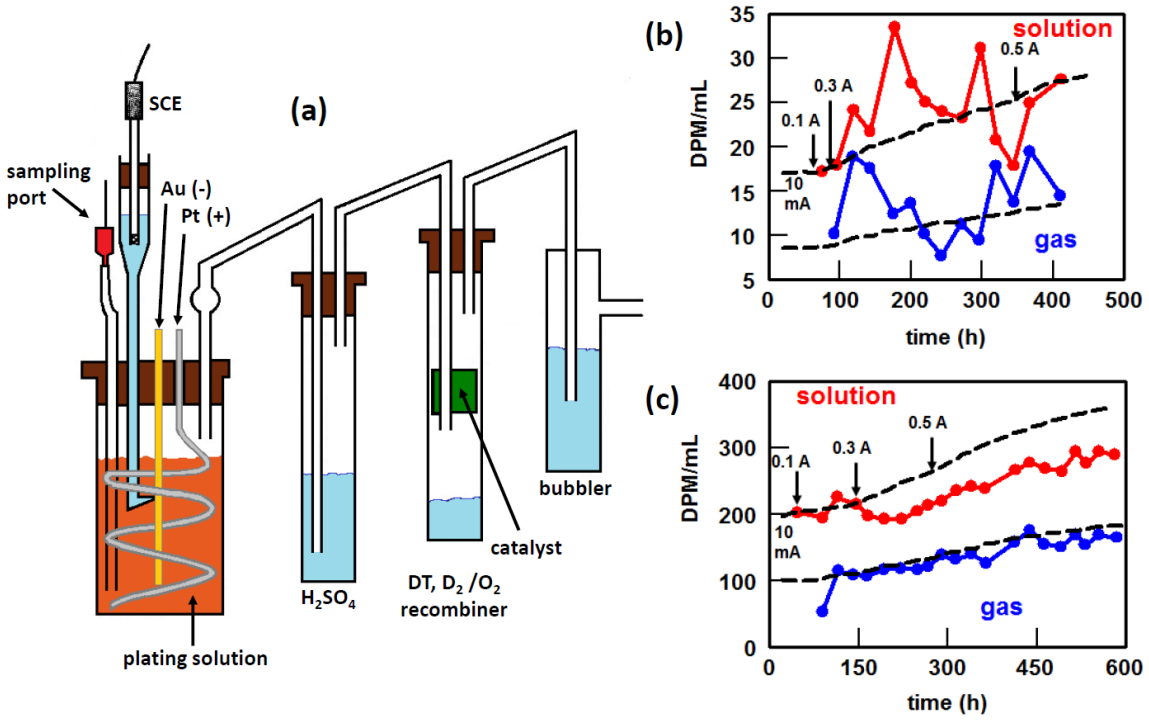

Figure 1. (a) Schematic of the experimental apparatus used by Bockris *et al.* to determine tritium content in both the gas and liquid phases [2]. Amount of tritium measured in the gas and liquid phases for experiments using (b) low tritiated D_2O and (c) highly tritiated D_2O. Current changes are indicated. Dashed lines are the expected amount of tritium based on the mass balance and isotopic separation factor, S = 0.63.

2. Summary of Pd/D Co-Deposition Tritium Results

2.1. John O'M Bockris *et al.*

Figure 1a shows a schematic of the experimental set-up for Pd/D co-deposition with simultaneous measurements of tritium in the liquid and gas phases [2]. The anode and cathode are in a concentric orientation. It is an open system using a $PdCl_2$-LiCl plating solution. The resultant Pd deposit on the Au cathode was thick and dendritic. Concentrated sulfuric acid was used as a trap for solution vapors. The D_2/DT and O_2 gases were recombined on a C-supported Pt catalyst. A bubbler at the end assured that the whole system was isolated from the atmosphere. The scintillation technique was used to measure the tritium content in both gas and liquid phases. Experiments typically ran for two weeks. Periodically fresh D_2O would be added to the electrolyte to replenish what was electrolyzed. In this methodology, a change in tritium concentration in the liquid phase occurs due to the addition of fresh D_2O containing background levels of tritium and due to the removal of tritium by electrolysis. Figures 1b and c summarize the observed results. Tritium production was observed when low tritiated D_2O was used, Figure 1b. A burst of tritium production was observed in the gas phase. At the same time, or with a slight delay, a burst of tritium would occur in the liquid phase. When highly tritiated D_2O was used, no excess of tritium was observed, Figure 1c. Instead, a loss of tritium was observed, primarily in the electrolyte. For the most part, the measured and calculated tritium values in the gas phase are in agreement. No explanation for this loss was presented.

Table 1. Summary of tritium results obtained by Miles using an open system [5].

Cathode	D_2O Consumption (mL)	Tritium (DPM ml^{-1})
D_2O	N/A	223.74 ± 0.89
Pd, cell A	161.0	361.26 ± 1.12
Pd, cell B	175.0	347.02 ± 1.11
Pd-Ce-B	248.5	336.92 ± 1.08
Pd-Ce	258.0	334.92 ± 1.07
Pd/D co-deposition cell A	7.4 ± 1.0	217.24 ± 0.87
Pd/D co-deposition cell B	7.7 ± 1.0	212.62 ± 0.87
Pd/D co-deposition cell C	8.7 ± 1.0	214.21 ± 0.89

2.2. Mel Miles

In experiments using bulk cathodes and Pd/D co-deposition, Miles used an open system with the electrodes in a concentric orientation [5]. He used highly tritiated D_2O. For Pd/D co-deposition, the cathode was copper and the plating solution was $PdCl_2$ – ND_4Cl – ND_4OD. This plating solution was chosen to produce a smooth, bright deposit; however, the resultant deposit was dark and dendritic. Liquid scintillation technique was used to measure tritium at the end of the experiment on the final electrolyte solutions after adjusting the D_2O levels to the initial volumes. Results are summarized in Table 1. For bulk cathodes an increase in tritium was observed that was attributed to enrichment as a result of electrolysis. However, the Pd/D co-deposition cells showed a decrease in tritium. It should be noted that all three of the Pd/D co-deposition cells produced excess heat and showed the positive feedback effect [1], [7].

2.3. P.A. Mosier-Boss and S. Szpak

A schematic of the apparatus used by Mosier-Boss and Szpak [4] to measure tritium in the gas and liquid phases is shown in Figure 2a. The anode and cathode are in a concentric orientation. A catalyst in a separate chamber is used to recombine the D_2 (DT) and O_2 gases. Five experiments were done using low tritiated D_2O and a $PdCl_2$-LiCl plating solution that produced a dark, mossy deposit on a Ag plated Cu cathode. Figures 2b and c show plots of the measured tritium content and the expected amount of tritium which was calculated using the following equation:

$$f(t) = f(0)\left(\frac{m(0) - r(i)t}{m(0)}\right)^{S-1} + \frac{q}{(S-1)r(i)} \bullet \left\{1 - \left[\frac{m(0) - r(i)t}{m(0)}\right]^{S-1}\right\}$$

where t = time; f = tritium mass fraction; m = mass of the electrolyte phase; $r(i) = iM_w/2F$ = the rate of change associated with the passage of cell current i; q = rate at which tritium is added/removed from the solution phase by whatever process including transport of tritium generated on the bulk electrode; and s = isotopic separation factor $= (C_T/C_D)_g/(C_T/C_D)_l$ where C is concentration, T is tritium, D is deuterium, g is gas, and l is liquid. Two experiments showed a complete mass balance as shown in Figure 2b. Three showed excess tritium, Figure 2c. Tritium production was sporadic and occurred in bursts, as was observed by Bockris *et al.* [2]. During a burst, the rate of tritium production ranged between 3000-7000 atoms s^{-1} for a 24 h period.

2.4. K.-H. Lee *et al.*

Lee *et al.* [6] used a closed system to measure changes in tritium content in cells using bulk Pd and Pd/D co-deposition, Figure 3a. The electrodes were parallel to one another. Two kinds of plating solutions were used for Pd/D co-deposition – $PdCl_2$-LiCl and $Pd(en)Cl_2$-LiCl, where en is ethylene diamine. Both low and highly tritiated D_2O were used. The scintillation technique was used to measure the tritium content of the electrolyte before and after the experiment.

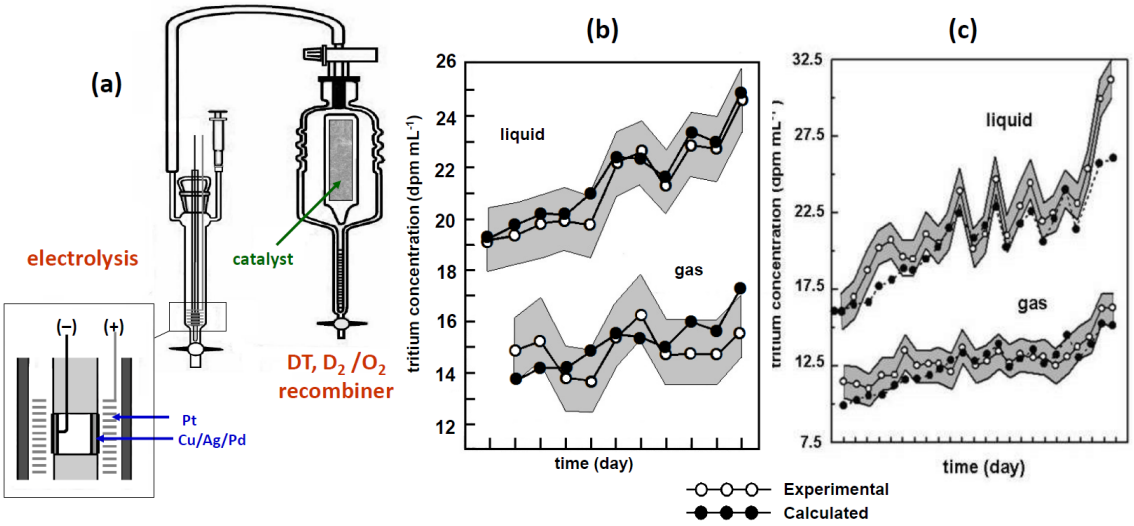

Figure 2. (a) Schematic of the experimental apparatus used by Mosier-Boss and Szpak to determine tritium content in both the gas and liquid phases [4]. Tritium content was measured using the scintillation technique. Results of two experimental runs showing (b) no tritium production and (c) tritium production occurring in bursts. The isotopic separation factor, s, was 0.68 ± 0.04, which is in agreement with the value determined by Bockris *et al.* [2].

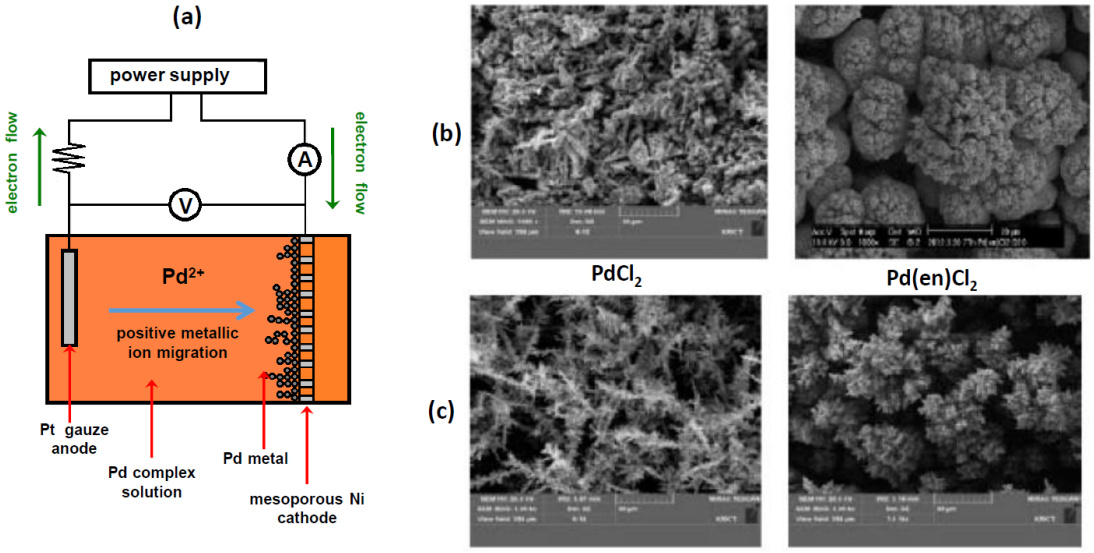

Figure 3. (a) Schematic of the experimental apparatus used by Lee *et al.* [6]. This is a closed system. Tritium content of the electrolyte was measured before and after completion of the experiment. SEM images of the deposits formed using $PdCl_2$ and $Pd(en)Cl_2$ salts when (b) highly tritiated and (c) low tritiated D_2O were used.

Table 2. Summary of tritium results obtained by Lee *et al.* using a closed system [6].

cathode, electrolyte, and cathodic charging profile[a-c]	tritium before electrolysis (CPM)	tritium after electrolysis (CPM)
Pd foil, LiCl, i = 20-400 mA for 65 h	10.00	167.00
mesoporous Ni, $PdCl_2$-LiCl, i = 1 mA for 168 h	40.00	35.00
mesoporous Ni, $PdCl_2$-LiCl, i = 20-400 mA for 65 h	28.00	314.00
mesoporous Ni, $PdCl_2$-LiCl, i = 1-300 mA for 97 h	596.00	235.00
mesoporous Ni, Pd(en)Cl_2-LiCl, i = 1 mA for 168 h	24.00	26.00
mesoporous Ni, Pd(en)Cl_2-LiCl, i = 1-300 mA for 97 h	30.00	258.00
mesoporous Ni, Pd(en)Cl_2-LiCl, i = 1-200 mA for 77 h	489.00	160.00

a. en is ethylene diamine
b. $PdCl_2$ and Pd(en)Cl_2 complexes were in ammonia water
c. All electrolytes were in D_2O.

Results are summarized in Table 2. For the bulk Pd cathode, tritium production was observed using low tritiated D_2O. No results were reported for highly tritiated D_2O. For Pd/D co-deposition, no change in tritium was observed using both complexes and low tritiated D_2O when a current of -1 mA was applied for 168 h. However, when the current was increased, excess tritium was observed which agreed with the results obtained by Bockris *et al.* [2], [3] and Szpak *et al.* [4]. Furthermore, Pd/D co-deposition produced more tritium than electrolysis using a bulk cathode. When highly tritiated D_2O was used, Pd/D co-deposition using both complexes resulted in a decrease in tritium content. These results agreed with the observations of Bockris *et al.* [2], [3] and Miles [5]. Lee *et al.* also obtained SEM images of the deposit formed using both complexes in highly tritated, Figure 3b, and low tritiated D_2O, Figure 3c [6]. It can be seen that the deposits exhibit a highly fractal surface.

3. Determining the Reactions Responsible for the Consumption of Thermal (0.025 eV) Tritium

Four groups conducted experiments measuring tritium in Pd/D co-deposition experiments. In each experiment, the Pd deposit was black and dendritic with high surface area. Different plating solutions and cathode substrates were used. Three groups had a concentric orientation for their anode and cathode while one had a parallel arrangement. Three used open systems while one used a closed one. Regardless of the experimental configuration employed, tritium production was observed when low tritiated D_2O was used. In contrast, when highly tritiated D_2O was used a decrease in tritium was observed. During electrolysis, both D and T will partition into the Pd lattice regardless of the D_2O used (low or highly tritiated). More T will enter the lattice when highly tritiated D_2O is used than low tritiated. The D and T that partition into the Pd lattice are thermalized. Under conditions of high D/Pd loading and D flux in the lattice, LENR is initiated. The exact mechanism of how this occurs is not understood and there are a number of theories. It is not the scope of this communication to elucidate what this mechanism is but rather to determine what happens after it occurs. Specifically, the decrease in tritium that occurs when highly tritiated D_2O is used suggests that there is a nuclear reaction(s) that consumes thermal tritium. In Pd/D co-deposition, we have Pd and Li salts present as well as D_2O. We began to examine nuclear reactions that can occur between T and solution components (Pd, D, ^{6}Li, and ^{7}Li) as well as reactions between T and nuclear generated particles (P, T, ^{3}He, and ^{4}He).

3.1. Possible Nuclear Reactions Between Either Li or Pd Isotopes and Tritium

The standard approach to measuring nuclear reaction cross sections is to have a beam of ions (with well-defined ion species, current, and kinetic energy) impinge on a sample that contains the target nuclei of known density. Nuclear diagnostics are used to detect/quantify reaction products normal to the beam over a 2π angle. There are no cross

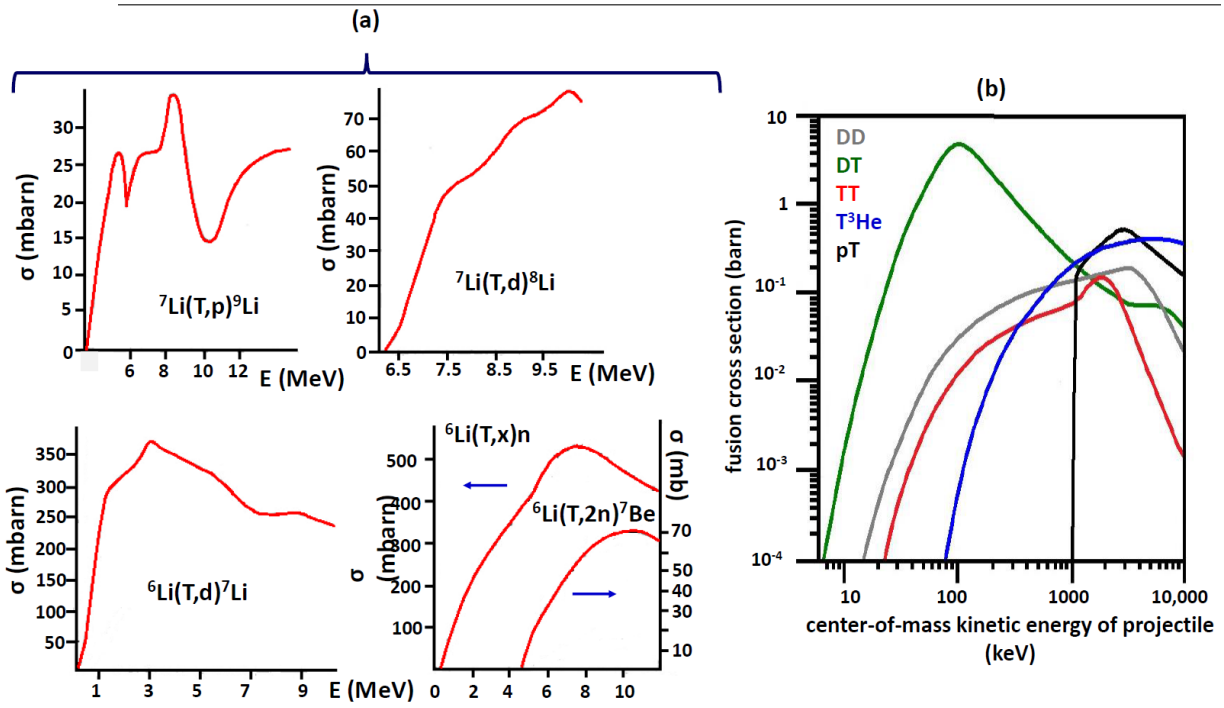

Figure 4. (a) Plots of the representative Li-T nuclear reaction cross sections [9]. (b) Standard cross-sections for the primary hot fusion reactions as a function of projectile energy [10]. Not shown is the cross section of the T-^{4}He reaction as a function of projectile energy. As shown in Table 3, the maximum cross section, σ_{max}, of this reaction is 3.58 μbarn.

sections reported for Pd(t,x)y reactions so nuclear reactions between Pd isotopes and tritium cannot account for the observed loss of thermal tritium. Also if such reactions did occur, it would involve energetic T and not thermal T.

Cyclic voltammetry measurements have shown that electrochemical incorporation of lithium into palladium can occur [8]. So nuclear reactions between Li and T may be possible inside the Pd lattice. There are a number of nuclear reactions between tritium and ^{6}Li/^{7}Li isotopes and the reaction cross sections are in millibarns [9]. Figure 4a shows plots for Li-T reactions exhibiting the largest cross sections. Although there are measurable nuclear cross sections for Li-T interactions, these interactions involve energetic T. Furthermore, Miles [5] observed a decrease in tritium content when he used highly tritiated D_2O and his electrolyte did not contain lithium salts. Therefore, it is unlikely that the reaction that consumes tritium involves Li isotopes.

3.2. Possible Nuclear Reactions Between Either ^{n}H or ^{n}He Isotopes and Tritium

Standard cross-sections for the fusion reactions between tritium and ^{n}H or ^{n}He isotopes as a function of projectile energy are shown in Figure 4b [10]. The maximum cross section, σ_{max}, and its energy, ε_{max}, for each T-^{n}H and T-^{n}He reaction are tabulated in Table 3. These cross-sections, and the screening potentials discussed below, relate to hot fusion reactions. However, in the Pd/D system, there have been reports of the production of energetic charged particles *in-situ* [16-21]. These charged particles will traverse through the Pd/D lattice, which is analogous to the charged particle projectiles used in the ion bombardment experiments to measure nuclear cross sections and electron screening.

Table 3. Fusion reactions: maximum cross section σ_{max} and location of the maximum ε_{max} [9]–[15].

Nuclear Reaction	σ_{max} **(barn)**	ε_{max} **(keV)**
D + T → α (3.52 MeV) + n (14.06 MeV)	5.0	64
D + D → T (1.01 MeV) + p (3.02 MeV) 50%	0.096	1250
D + D → ^{3}He (0.82 MeV) + n (2.45 MeV) 50%	0.11	1750
T + T → α + 2n+ 11.3 MeV	0.106	1000
T + ^{3}He → α + p + n + 12.9 MeV 57%	0.5	5000
T + ^{3}He → α (4.8 MeV) + D (9.5 MeV) 43%		
p + T → ^{3}He + n	0.6	3000
T + ^{4}He → ^{7}Li + γ	3.58x10^{-6}	1320

Consequently, use of the data summarized in Figure 4b and Table 3 are applicable to determine what reactions are responsible for the loss of thermal tritium. Looking at Table 3, the T(α,γ)^{7}Li can be ruled out as being responsible for causing the loss of tritium as the maximum cross section for this reaction is 3.58 $\pm$ 0.60 microbarns [15], which is between five and six orders of magnitude lower than the other T-^{n}H and T-^{3}He reactions.

Of the reactions summarized in Table 3, we have seen evidence of the DT reaction using a solid-state nuclear track detector (SSNTD), CR-39. This reaction has a maximum cross section of 5 barns, Table 3, and creates 14.06 MeV neutrons. Columbia Resin 39, or CR-39, is a clear, amorphous, thermoset plastic that is used to detect nuclear particles [22]. When an energetic charged particle traverses through CR-39, it creates along its path an ionization trail that is more sensitive to chemical etching than the bulk material. After treatment with a chemical etchant, tracks due to energetic particles remain in the form of holes or pits which can be examined with the aid of an optical microscope. The size, depth of penetration, and shape of the track provides information about the mass, charge, energy, and direction of motion of the particle that created the track [23]. Besides charged particles, CR-39 can also be used to detect neutrons. In particular, triple tracks are diagnostic of the 14 MeV neutrons. When a 14 MeV neutron collides with a carbon atom in CR-39, it can either cause the carbon atom to recoil or it can shatter it into three alpha particles. After etching, these three alpha particles appear in CR-39 as three particle tracks breaking away from a center point, *i.e.*, a triple track. Such triple tracks have been observed in CR-39 used in Pd/D co-deposition experiments [24]. Figure 5a compares Pd/D co-deposition generated triple tracks in CR-39 detectors with those produced by exposing detectors to an accelerated driven, DT neutron source [25]. As can be seen the Pd/D co-deposition generated triple tracks are similar to the DT neutron generated tracks. The tracks shown in Figure 5a do not have the same exact shape and the lobes making up the triple tracks do not necessarily need to have the same size. This is because the n + ^{12}C breakup reaction can proceed to the four-body final state through one or more of the reaction mechanisms shown in Figure 5b [26]. Although the DT reaction will consume tritium, the energy of the triton needs to be $\geq$ 5 keV [27] and is therefore energetic. However, the tritium lost in the highly tritiated D_2O experiments is thermal. Electron screening may lower this threshold.

Screening effects in gases, solids, and dense plasmas (metal hydrides are considered to be cold dense plasmas [28]) can increase fusion rates at low reaction energies by several orders of magnitude because screening of the repulsive Coulomb potential by plasmas or target atom electrons increases the probability for ions to tunnel through the Coulomb barrier [29, 30]. The electron screening effect can be expressed as a screening potential, U_e. The value of the screening potential strongly depends on the electronic properties of the host material [29]. The mechanism of electron screening is not fully understood and not all of the contributing factors are known. It is known that the screening potential caused by electrons in gaseous plasma is only several tens of eV for the DD fusion reaction [24], yet is as much as 20 orders of magnitude higher in deuterated metals [28]. There is a strong correlation between the screening potential and the

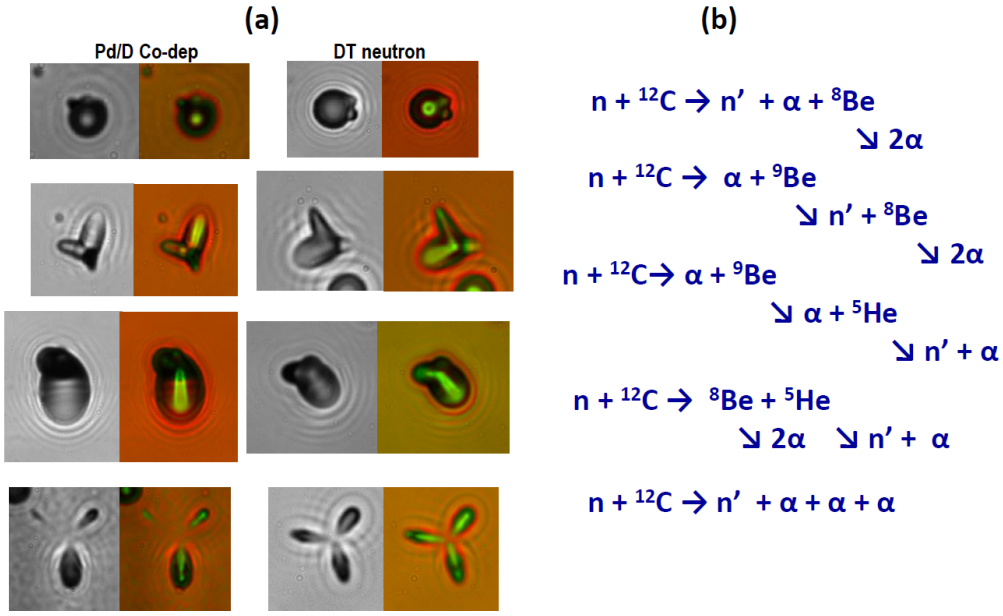

Figure 5. (a) Comparison of triple tracks observed in CR-39 detectors used in Pd/D co-deposition experiments and in detectors exposed to DT neutrons [25]. For both sets of tracks, the left-hand images were obtained with the microscope optics focused on the surface of the CR-39 detector while the right-hand images are an overlay of two microphotographs taken at different focusing depths (surface of the detector and the bottom of the pits). (b) Summary of the n + ^{12}C breakup reaction mechanisms.

deuteron density in metal during the bombardment. The deuteron density during the bombardment is inversely related to the fluidity of the deuteron. Kasagi *et al*. [31, 32] have postulated that a fluidity of deuterons in metals contributes to a reduction of the Coulomb barrier between the fusing nuclei. Pines has noted that this gives rise to plasma screening [28] likely enhanced at the Bragg Peak for the accelerated deuterons. Schenkel *et al.* [30] has argued that U_e is likely dependent on details of target loading and defect dynamics.

Table 4 summarizes screening potentials that have been measured for several Pd species. It can be seen that significantly higher enhancements have been observed for PdLi alloys. For the $PdLi_{0.1\%}$ alloy, a screening potential of ~ 4 keV has been measured for the ^{7}Li(p,α)α reaction. While Bockris *et al.* [2], Szpak and Mosier-Boss [4], and Lee *et al.* [6] used lithium salts in their electrolytes and lithium can intercalate into the Pd lattice, Miles [5] had no lithium in his electrolyte and he still observed a decrease in tritium. This would suggest that the 5 keV energy requirement is unattainable for DT fusion to occur to consume thermal tritium. However, care must be taken in using the cross sections summarized in Figure 4b and Table 3 as they have been obtained for hot fusion reactions that occur under conditions (ion density, confinement time, temperature) that make electron screening effects negligible. It is therefore very possible that, when electron screening is taken into account, the threshold energies for these reactions in metal hydrides may actually be lower than those shown in Figure 4b for hot fusion reactions. If so, then the electron screening could be sufficient to allow DT reactions to occur in the metal lattice that consume thermal tritons.

We next consider the TT and T^{3}He secondary fusion reactions. In the TT reaction, energetic tritons formed from DD reactions will consume both thermal and energetic tritium. Using NE213 neutron detectors, CR-39, and SSB detectors, Lipson *et al.* [18] obtained evidence of energetic protons, tritons, and 2.45 MeV neutrons. They attributed

Table 4. Screening potential energies for Pd species.

Target	Reaction	Screening Potential, U_e (eV)
Pd [30]	D(d,n)^{3}He	1000 ± 250
Pd [31]	D(d,p)T	310 ±20
PdO [31]	D(d,p)T	600 ± 20
Pd [32]	^{6,7}Li(d,α)^{4,5}He	1500 ± 310
$PdD_{0.2}$ [33]	D(d,p)T	296 ± 15
$PdLi_{1\%}$ [34]	^{6}Li(p,α)^{3}He	3760 ± 260
$PdLi_{1\%}$ [34]	^{7}Li(p,α)α	3790 ± 330
$PdLi_{0.1\%}$ [34]	^{7}Li(p,α)α	4100 ± 650

formation of these particles to DD fusion reactions occurring inside the lattice. The group in SRI had conducted Pd/D co-deposition experiments using CR-39 detectors both immersed in the electrolyte and outside the cell [35], [36]. In the latter experiments, a 6 μm Mylar film separated the cathode and the detector. Roussetski *et al.* [36] did sequential etching analysis of these detectors. Tracks due to proton recoils caused by neutrons were detected. The energy of these neutrons was on the order of 2.45 MeV, Figure 6a. Direct detection of ^{3}He was not possible as it would be difficult to differentiate alpha and ^{3}He tracks. Consequently, in both the Lipson *et al.* [18] and the SRI experiments [35], [36], the presence of 2.45 MeV neutrons infers that ^{3}He particles were created but could not be directly detected. However, the D(^{3}He,p)α original and downscattered 14.7 MeV protons have been observed indicating the production of ^{3}He [35].

For a 1.01 MeV triton, the cross section of the TT reaction, not taking into account electron screening, is 89 mbarn. SRIM [37] can be used to calculate how far a charged particle can travel through a medium. Using SRIM, a 1.01 MeV triton will traverse 4.86 μm of PdD, which is equivalent to 11,916 unit cells. The TT reaction will result in some loss of thermal tritons but is probably not the primary reaction. The ^{3}He formed from DD reactions has an energy of 0.82 MeV. This energetic ^{3}He ion will react with thermal tritons. For a 0.82 MeV ^{3}He, the cross section of the T^{3}He reaction is 189 mbarn. However, SRIM calculations indicate that a 0.82 MeV ^{3}He will traverse only 1.15 μm of PdD, or 2,813 unit cells. The T^{3}He secondary fusion reaction forms either a 9.5 MeV deuteron and a 4.8 MeV alpha (43% of the time) or a proton, alpha, and a neutron (57% of the time). The 9.5 MeV deuteron, formed 43% of the time, can undergo more DD reactions to form more energetic ^{3}He ions and tritons. A 9.5 MeV deuteron will pass through 133.61 μm of PdD, or 327,479 unit cells. Although the T^{3}He reaction will eliminate thermal tritons, given the cross section and how far the ^{3}He ions can travel through the PdD lattice, this reaction is not the main reaction responsible for the loss of tritium.

The pT reaction involves a thermal triton and a high energy proton so thermal tritons will be consumed. There are two sources of energetic protons. One is the DD primary fusion reaction to form a 3.02 MeV proton and a 1.01 MeV triton. The other is the ^{3}HeD secondary fusion reaction that produces 14.7 MeV protons and 3.6 MeV alpha particles. Pd/D co-deposition experiments using CR-39 detectors have shown that both 3.02 and 14.7 MeV protons have been produced [35, 36]. Roussetski *et al.* [36] had subjected a CR-39 detector used in a co-deposition experiment to destructive sequential etching analysis. The results, shown in Figure 6b, showed tracks attributed to 3 MeV protons, 12 MeV alpha, and 16 MeV alphas. Prior to the destructive sequential etching analysis, this same detector had been scanned using a TASL Image system [38] to obtain quantitative information on the pits produced in the CR-39 detector [35]. Fifteen characteristic measurements of each feature in the detector are made to reliably discriminate between etched tracks and background blemishes in the plastic detectors. These measurements include track length and diameter, optical density (average image contrast), and image symmetry. Based upon the measured properties of a feature, the software algorithm determines whether or not those measurements are consistent with that

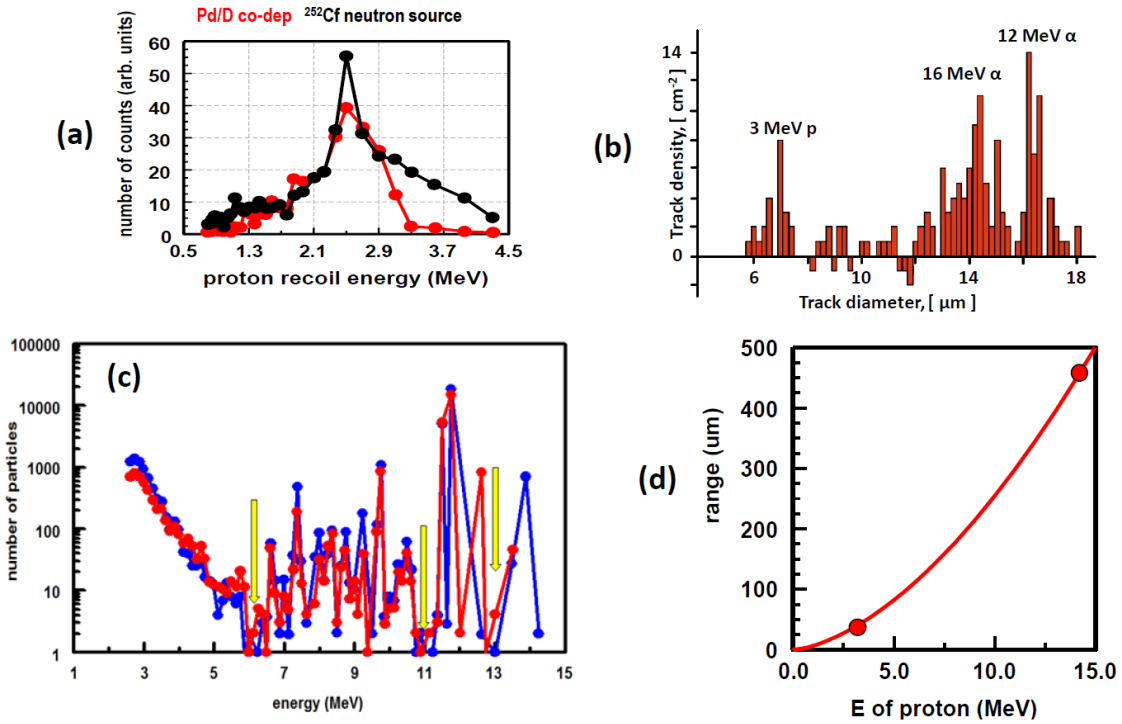

Figure 6. (a) Reconstruction of the protons recoil spectra from both Pd/D co-deposition and ^{252}Cf exposure [36]. The detector used in Pd/D co-deposition was from a non-immersion experiment where a 6 μm Mylar window separated the cathode from the detector. The detector had been etched for 14 h. (b) The difference between the nuclear track distribution on the front side of a detector in direct contact with the Ag/Pd cathode and the neutron induced proton recoil track distribution on the back side. [36]. The detector had been etched for 21 h. (c) Energy distribution of protons on the side of detectors in contact with the Ag/Pd cathodes [35]. Linear energy transfer (LET) analysis was used to determine the energies of the protons. Troughs in the energy distribution, indicated with ↓, suggest that protons with these energies are being consumed. (d) LET curve calculated for protons traversing through PdD. The 3.02 and 14.7 MeV protons are indicated (●).

of an energetic particle. LET analysis using the scanned data obtained for the detectors was done [35]. The tracks on detector surface in contact with the cathode were identified as $\geq$ 1.8 MeV protons, $\geq$ 1.8 MeV alphas, and secondary particles due to recoils from either energetic protons and/or neutrons. The energy distribution of the protons, Figure 6c, shows the presence of both 3.02 MeV and 14.7 MeV protons. Arrows indicate troughs at 6, 11, and 13 MeV which indicate that protons of these energies are being used up in additional nuclear reactions. Protons with energies between 5 and 20 MeV will cause palladium to transmute to silver [1]. SEM/EDX analysis of a cathode used in a Pd/D co-deposition experiment, Dash and Ambadkar saw evidence of Ag production [39], [40].

In the pT reaction, a 3.0 MeV proton has a cross section of 600 mbarn, which is significant. A SRIM calculation was done and the results are shown in Figure 6d. This calculation shows that a 3.02 MeV proton will pass through 34.29 μm of PdD, or 84,052 unit cells. A 14.7 MeV proton will traverse 433.43 μm of PdD. This is equivalent to 1,062,339 unit cells. Given the cross sections of the reaction and the distances the energetic protons can travel through PdD, the pT reaction is primarily responsible for the loss of tritium.

4. Conclusions

For Pd/D co-deposition, it has been demonstrated that tritium production occurs when low tritiated D_2O is used. When tritium is produced, it occurs in bursts and sporadically. In contrast, a loss of tritium is observed when highly tritiated D_2O is used. The loss of tritium indicates that reactions are occurring inside the lattice that consumes thermal tritium. Nuclear reactions involving tritons with Pd and Li isotopes were examined. No cross sections were found for T^nPd reactions. While there are a number of T^nLi nuclear reactions with cross sections in the millibarns, Mel Miles [5] did not use electrolytes containing lithium salts and he still observed a loss of tritium. Therefore, the reactions resulting in a decrease in tritium does not involve Li and Pd isotopes.

Reactions between tritium and hydrogen and helium isotopes were then explored. Because the maximum cross section for the T^4He is 3.58 μbarn, this reaction is not responsible for the observed decrease in thermal tritium when highly tritiated D_2O is used. The DT reaction has a maximum cross section of 5 barn; however, the triton has to be energetic. For hot fusion, the threshold energy for the triton is 5 keV. But the conditions (ion density, confinement time, temperature) of hot fusion are not the same as those in LENR. Metal hydrides/deuterides are essentially cold, dense plasmas [28] conducive to electron screening effects that would lower that energy threshold. It should be noted that triple tracks have been observed in CR-39 detectors used in Pd/D co-deposition experiments. These triple tracks are diagnostic of 14 MeV neutrons likely resulting from DT fusion. Given the exceptionally high cross sections for the DT reaction and electron screening, it is possible that thermal tritons are consumed. However, it is probably not the primary reaction responsible for the observed loss of tritium when highly tritiated D_2O is used.

The TT reaction will consume both thermal and energetic tritons. The T(T,2n)α is a three body reaction resulting in continuum neutron energies from 1-9 MeV, which are not observed. The DD reaction will produce 1.01 MeV tritons. For a 1.01 MeV triton, the cross section of the TT reaction is 89 mbarn and a 1.01 MeV triton can travel through 4.86 μm of PdD, which equates to 11,916 unit cells. The T^3He reaction will consume thermal tritons. The ^3He ion formed from the DD reaction has an energy of 0.82 MeV. A ^3He ion of this energy will have a cross section of 189 mbarn for the T^3He reaction. A 0.82 MeV ^3He ion will traverse 1.15 μm of PdD, or 2813 unit cells. In hot fusion, 43% of the time, the T^3He reaction will form 9.5 MeV D that will undergo additional DD reactions to generate more 0.82 MeV ^3He, 3.02 MeV p, and 1.01 MeV T that can interact with more thermal tritons. A 9.5 MeV D will go through 133.61 μm of PdD, or 327,479 unit cells. It should be pointed out that, while in hot fusion, the T/n branching ratio for the DD reactions is unity, in LENR the branching ratio is near 10^6 [41] meaning that the production of tritium is highly favoured. Although both the TT and T^3He reactions will consume thermal tritons, the TT reaction will contribute more to this loss but, based upon the cross sections of the reaction and how far a 1.01 MeV T can travel through PdD, it is unlikely to be the primary reaction responsible for the loss of thermal tritons.

The pT reaction was then examined. This reaction will react with thermal tritons. At 3.0 MeV, the cross section is 600 mbarn. Destructive sequential etching and LET analyses of CR-39 detectors used in Pd/D co-deposition experiments showed the presence of tracks due to 3.02 and 14.7 MeV protons [30], [31]. A 3.02 MeV p can travel through 23.29 μm of PdD. This is equivalent to 84,052 unit cells. In contrast a 14.7 MeV p traverses through 433.43 μm of PdD, or 1,062,229 unit cells which greatly increases the probability of a proton to encounter a triton in the lattice. Given the cross sections of reaction and the distance the protons can travel through PdD, the pT reaction is primarily responsible for the loss of thermal tritium observed when highly tritiated D_2O is used in Pd/D co-deposition experiments.

This loss of tritium when highly tritiated D_2O is used in electrolysis experiments had only been observed in Pd/D co-deposition. The difference in the behaviour of bulk Pd and the Pd deposit created as a result of co-deposition is illustrated in Figure 7, which shows photomicrographs of CR-39 obtained at 20x and 200x magnification. Figure 7a was obtained for a CR-39 detector used in a Pd/D co-deposition experiment. Not only is the density of tracks high, but tracks occur homogeneously where the Pd deposit on the Ag wire was in contact with the detector. In contrast,

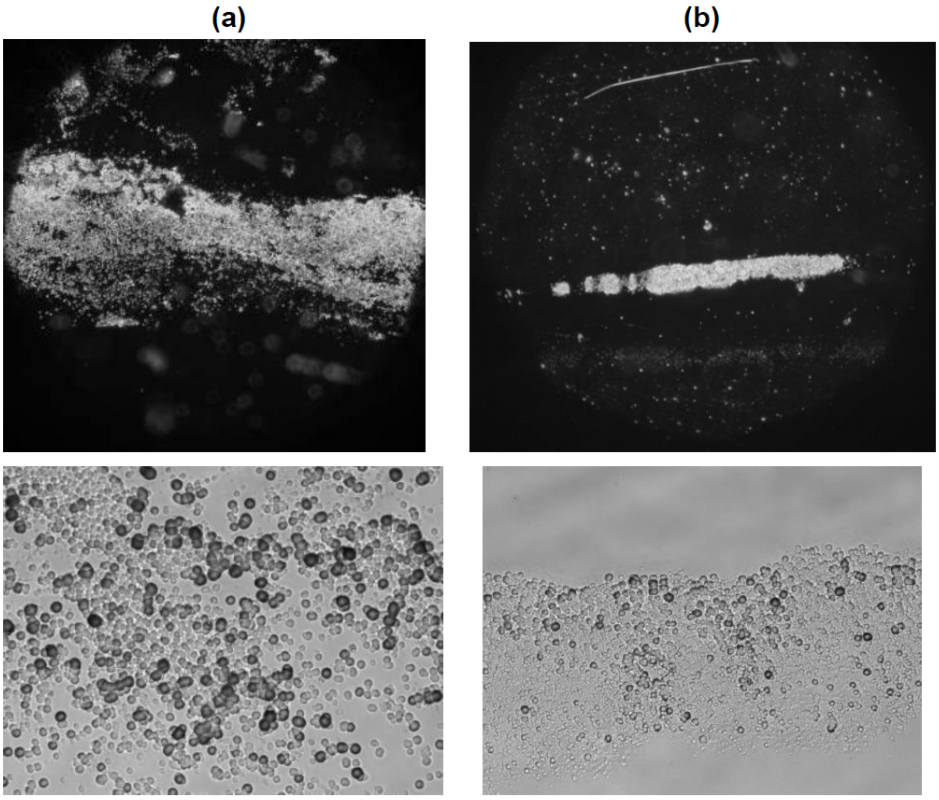

Figure 7. Photomicrographs obtained at 20x (top) and 200x (bottom) magnification for CR-39 detectors used in (a) Pd/D co-deposition in D_2O on a Ag cathode and (b) bulk Pd electrolysis in D_2O. The diameter of the Pd wire was 250 μm. The time duration of operation was the same for both experiments.

visual inspection of the CR-39 detector used in the bulk Pd wire experiment done in D_2O showed scattered cloudy areas in the detector along the length of the Pd wire. Figure 7b shows photomicrographs of one such cloudy area where the Pd wire was in contact with the detector. Although tracks are observed, the density of tracks is significantly less than that observed for the co-deposition experiment. This indicates that there are fewer active sites in bulk Pd than in the Pd deposit formed as a result of co-deposition. Figure 8a shows an SEM obtained for a Pd deposit on a Au foil cathode. The SEM is similar to those obtained by Lee *et al.* [6], Figures 3b and c. The deposit exhibits a high surface area and it will exhibit vacancies. The SEMs of the Pd deposit show that it is comprised of aggregates of Pd nm-μm sized globules. Akiba *et al*. [42] conducted neutron powder diffraction experiments on bulk and nanoparticles of palladium deuteride. Analysis showed that for nanocrystals, 30% of D atoms are located at the tetrahedral sites and 70% at the octahedral sites, shown schematically in Figure 8b. In contrast they found that only the octahedral sites of bulk Pd were occupied with D. This indicates > 1 D/Pd loadings for Pd nanoparticles. Earlier Szpak *et al.* showed high D loadings (D/Pd $\geq$ 1) in the Pd deposit using galvanostatic pulsing experiments [43]. Besides high D/Pd loadings, these vacancies will exhibit D flux [44]. Both the loading and the flux will increase the amount of electron screening [30]-[32] in the Pd deposit, compared to bulk Pd, and may account for the observed results.

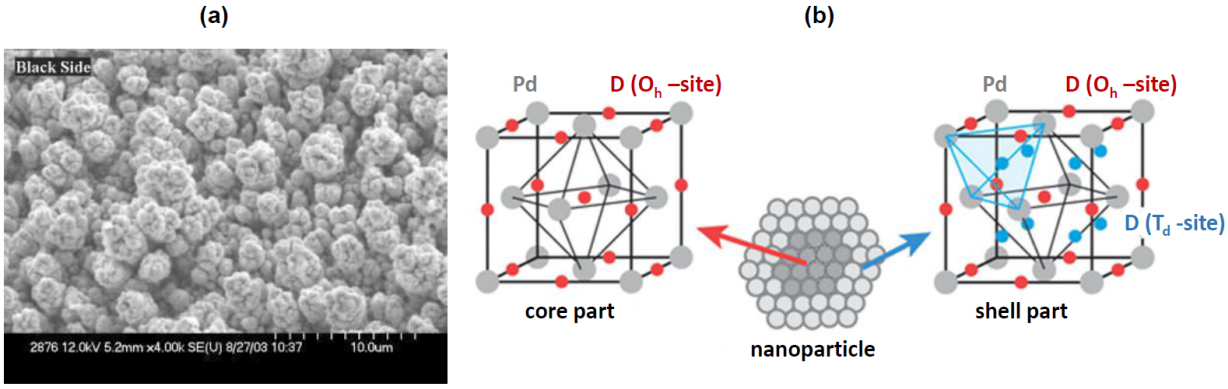

Figure 8. (a) SEM image of a Pd film deposited on Au foil. (b) Schematic showing the placement of deuterons in the lattice of a Pd nanoparticle (reproduced with permission from the J. Am. Chem. Soc. [42]).

5. Acknowledgements

The authors would like to thank the research groups who conducted Pd/D co-deposition experiments that focused on tritium measurements. They would like to thank Fran Tanzella and Ben Earle for replicating the CR-39 results and the late Andrei Lipson, Alexei Roussetski, and Dazhuang Zhou for analysing the detectors used in that replication. We are grateful to Dr. Frank Gordon for his support of the work while he was a department head at SSC-Pacific as well as the support from Dr. Jay W. Khim of GEC. Finally, we acknowledge the contributions of the late Dr. Stan Szpak for conceiving and developing the Pd/D co-deposition process.

References

[1] P.A. Mosier-Boss, L.P. Forsley, "Review of Pd/D Co-deposition" in Cold Fusion: Advances in Condensed Matter Nuclear Science, J.-P. Biberian (ed.), Elsevier Science (2020).
[2] D. Hodko, J. O'M. Bockris, "Possible Excess Tritium Production on Pd Codeposited with Deuterium," J. Electroanal. Chem., vol. 353, pp. 33–41 (1993).
[3] J. O'M. Bockris, C.-C. Chien, D. Hodko, Z. Minevski, "Tritium and Helium Production in Palladium Electrodes and the Fugacity of Deuterium Therein," Third International Conference on Condensed Matter Nuclear Science, Nagoya, Japan (1992).
[4] S. Szpak, P.A. Mosier-Boss, R.D. Boss, "On the Behavior of the Cathodically Polarized Pd/D System: Evidence for Tritium Production," Fusion Sci. Technol., vol. 33, pp. 38–51 (1998).
[5] M.H. Miles, NEDO Final Report – Electrochemical Calorimetric Studies of Palladium and Palladium Alloys in Heavy Water, University of La Verne (2004).
[6] K.-H. Lee, H. Jang, S.-J. Kim, "A Change of Tritium Content in D_2O Solutions During Pd/D Co-deposition, J. Condens. Matter Nucl. Sci. vol. 13, pp. 294–298 (2014).
[7] S. Szpak, P.A. Mosier-Boss, M.H. Miles, "Calorimetry of Pd + D Co-deposition," Fusion Sci. Technol. vol. 36, pp. 234–241 (1999).
[8] F. Dalard, M. Ulmann, J. Augustynski, P Selvam, "Electrochemical Incorporation of Lithium into Palladium from Aprotic Electrolytes," J. Electroanal. Chem. Vol. 270, pp. 445–450 (1989).
[9] S.N. Abramovich, B. Ya. Guzhovskij. V.A. Zherebtsov, A.G. Zvenigorodskij, Nuclear Physics Constants for Thermonuclear Fusion: A Reference Handbook, International Nuclear Data Committee, Moscow, U.S.S.R. (1989).

[10] R.H. Majeed, O.N. Oudah, "Achieving an Optimum Slowing-Down Energy Distribution Functions and Corresponding Reaction Rates for the (D + ^{3}He and T + ^{3}He) Fusion Reactions," AIP Conference Proceedings, vol. 1968, pp. 30048 (2018).
[11] S. Atzeni, J. Meyer-ter-Vehn, "Nuclear Fusion Reactions," in The Physics of Inertial Fusion: Beam Plasma Interaction, Hydrodynamics, Hot Dense Matter, Oxford University Press (2004).
[12] https://www.newworldencyclopedia.org/entry/Nuclear_fusion
[13] G.H. Miley, H. Towner, N. Ivich, "Fusion Cross Sections and Reactivities," Technical Report Number COO-2218-17 (1974).
[14] D. Testa, M. Cecconello, C. Schlatter, "The Dependence of the Proton-Triton Thermo-Nuclear Fusion Reaction Rate on the Temperature and Total Energy Content of the High-Energy Proton Distribution Function," Nucl. Fus., vol. 40, pp. 062004 (2009).
[15] G.M. Griffiths, J.B. Warren, R.A. Morrow, P.J. Riley, "The T(α,γ)^{7}Li Reaction," Canadian J. Phys., vol. 39, pp. 1397–1408 (1961).
[16] A.G. Lipson. A.S. Roussetski, G.H. Miley, E.I. Saunin, "Phenomenon of an Energetic Charged Particle Emission from Hydrogen/Deuterium Loaded Metals," Tenth International Conference on Cold Fusion, Cambridge, MA (2003).
[17] A.G. Lipson. A.S. Roussetski, G.H. Miley, C.H. Castano, "In-Situ Charged Particles and X-ray Detection in Pd Thin Film-Cathodes during Electrolysis in Li_2SO_4/H_2O," Ninth International Conference on Cold Fusion, Beijing, China (2002).
[18] A.G. Lipson, B.F. Lyakhov, A.S. Roussetski, T. Akimoto, T. Mizuno, N. Asumi, R. Shimada, S. Miyashita, A. Takahashi, "Evidence for Low-Intensity D-D Reaction as a Result of Exothermic Deuterium Desorption from Au/Pd/PdO:D Heterostructure," Fusion Technol., vol. 38, pp. 238–252 (2000).
[19] T. Matusomoto, "Observation of New Particles Emitted during Cold Fusion," Fusion Technol., vol. 18, pp. 356–360 (1990).
[20] R. Taniguchi, T. Yamamoto, S. Irie, "Detection of Charged Particles Emitted by Electrolytically Induced Cold Fusion," Jpn. J. Appl. Phys. Part 2 Lett., vol. 28, pp. L2021-L2023 (1989).
[21] R. Taniguchi, T. Yamamoto, S. Irie, "Fine Structure of the Charged Particle Bursts Induced by Water-D_2 Electrolysis," Bull. Univ. Osaka Prefect, Ser. A, vol. 39, pp. 233–244 (1990).
[22] B.G. Cartwright, E.K. Shirk, P.B. Price,"A Nuclear-Track-Recording Polymer of Unique Sensitivity and Resolution," Nucl. Instrum. Meth., vol. 153, pp. 457–460 (1978).
[23] D. Nikezic, K.N. Yu, "Formation and Growth of Tracks in Nuclear Track Materials," Mater. Sci. Eng. R, vol. 46, pp. 51–123 (2004)
[24] P.A. Mosier-Boss, S. Szpak, F.E. Gordon, L.P.G. Forsley, "Triple Tracks in CR-39 as the Result of Pd-D Co-deposition: Evidence of Energetic Neutrons," Naturwissenschaften, vol. 96, pp. 135–142 (2009).
[25] P.A. Mosier-Boss, J.Y. Dea, L.P.G. Forsley, M.S. Morey, J.R. Tinsley, J.P. Hurley, F.E. Gordon, "Comparison of Pd/D Co-deposition and DT Neutron Generated Triple Tracks Observed in CR-39 Detectors,"Eur, Phys. J. Appl. Phys., vol. 51, p. 20901 (2010).
[26] B. Antolkoviæ, Z. Dolenec, "The Neutron-Induced ^{12}C(n,n')3α Reaction at 14.4 MeV in a Kinematically Complete Experiment," Nucl. Phys. A, vol. 237, pp. 235–252 (1975).
[27] S.K. Murali, B.B. Cipiti, J.F. Santarius, G.L. Kulcinski,"Study of Fusion Regimes in an Inertial Electrostatic Confinement Device using the New Eclipse Disk Diagnostic," Phys. Plasmas, vol. 12, pp. 053111 (2006).
[28] V. Pines, M. Pines, A. Chait, B. M. Steinetz, L. Forsley, R.C. Hendricks, G. C. Fralick, T. L. Benyo, B. Baramsai, P. B. Ugorowski, M. D. Becks, R. E. Martin, N. Penney, C. E. Sandifer II, "Nuclear Fusion Reactions in Deuterated Metals", Phys Rev C, vol. 101, p. 044609 (2020).
[29] M. Lipoglavšek, U. Mikac, "Electron Screening in Metals," AIP Conference Proceedings, vol. 1377, pp. 383 (2011).
[30] T. Schenkel, A. Persaud, H. Wang, P.A. Seidl, R. MacFadyen, C. Nelson, W.L. Waldron, J.-L. Vay, G. Deblonde, B. Wen, Y.-M. Chiang, B.P. MacLeod, Q. Ji, "Investigation of Light Ion Fusion Reactions with Plasma Discharges," J. Appl. Phy., vol. 126, pp. 203302 (2019).
[31] J. Kasagi, H. Yuki, T. Baba, T. Noda, "Low Energy Nuclear Fusion Reactions in Solids," Eighth International Conference on Condensed Matter Nuclear Science, Lerici, Italy (2000).
[32] J. Kasagi, H. Yuki, T. Baba, T. Noda, J. Taguchi, M. Shimokawa, W. Galster, "Strongly Enhanced Li + D Reaction in Pd Observed in Deuteron Bombardment on $PdLi_x$ with Energies between 30 and 75 keV," J. Phys. Soc. Japan, vol. 73, pp. 608–612 (2004).

[33] K. Czerski, A. Huke, P. Heide, G. Ruprecht, "The ^{2}H(d,p)^{3}H Reaction in Metallic Media at Very Low Energies," Europhys. Lett., vol. 68, pp. 363–369 (2004).
[34] J. Cruz, Z. Fülöp, G. Gyürky, F. Raiola, A. Di Leva, B. Limata, M. Fonseca, H. Luis, D. Schürmann, M. Aliotta, H.W. Becker, A.P. Jesus, K.U. Kettner, J.P. Ribeiro, C. Rolfs, M. Romano, E. Somorjai, F. Strieder, "Electron Screening in ^{7}Li(p,α)α and ^{6}Li(p,α)^{3}He for Different Environments," Phys. Lett. B, vol. 624, pp. 181–185 (2005).
[35] P.A. Mosier-Boss, F.E. Gordon, L.P. Forsley, D. Zhou, "Detection of High Energy Particles using CR-39 Detectors Part 1: Results of Microscopic Examination, Scanning, and LET Analysis," Int. J. Hydrogen Energy, vol. 42, pp. 416–428 (2017).
[36] A.S. Roussetski, A.G. Lipson, E.I. Saunin, F. Tanzella, M. McKubre, "Detection of High Energy Particles using CR-39 Detectors Part 2: Results of In-depth Destructive Etching Analysis," Int. J. Hydrogen Energy, vol. 42, pp. 429–436 (2017).
[37] J. Ziegler, http://www.srim.org/
[38] "Track Analysis Systems Ltd. Napier House. Meadow Grove, Shirehampton, Bristol, BS11 9PJ, UK Tel: +44 (0) 117 9381172; Website: info@tasl.co.uk
[39] J. Dash, A. Ambadkar, "Co-deposition of Palladium with Hydrogen Isotopes," Eleventh International Conference on Condensed Matter Nuclear Science, Marseille, France (2004).
[40] J. Dash, D.S. Silver, "Surface Studies after Loading Metals with Hydrogen and/or Deuterium," Thirteenth International Conference on Condensed Matter Nuclear Science, Sochi, Russia (2007).
[41] E. Storms, "A New Source of Energy using Low-Energy Fusion of Hydrogen," Environmental Science: An Indian Journal, vol. 13, pp. 1–7 (2017).
[42] A. Akiba, M. Kofu, H. Kobayashi, H. Kitagawa, K. Ikeda, T. Otomo, O. Yamamuro, "Nanometer-Size Effect on Hydrogen Sites in Palladium Lattice," J. Am. Chem. Soc., vol. 138, pp. 10238–10243 (2016).
[43] S. Szpak, P.A. Mosier-Boss, J.J. Smith, "Deuterium Uptake during Pd/D Co-deposition," J. Electroanal. Chem. Vol. 379, pp. 121–127 (1994).
[44] M.R. Staker, "Coupled Calorimetry and Resistivity Measurements in Conjunction with an Emended and More Complete Phase Diagram of the Palladium-Isotopic Hydrogen System," J. Condensed Matter Nucl. Sci., vol. 29, pp. 129–168 (2019).